

He-Si(100) potential: Charge superposition and model structures

A. Sakai,* M. J. Cardillo, and D. R. Hamann
AT&T Bell Laboratories, Murray Hill, New Jersey 07974
 (Received 7 October 1985)

We have studied the He-Si(100) scattering potential by considering the charge densities associated with different tilted dimer model structures. We demonstrate the inadequacy of spherical charge superposition schemes and develop an alternative procedure [modified atomic charge superposition (MACS)] which is calibrated against self-consistent linear-augmented-plane-wave charge densities. We demonstrate the transferability of the underlying MACS parameters for different periodicities of tilted dimer models of the Si(100) surface. We show that tilted dimer models of the Si(100) surface are consistent with experimental He diffraction data only if they are in an alternating $c(4 \times 2)$ array.

I. INTRODUCTION

The diffraction of He atoms from crystalline surfaces is developing into a powerful method to study the topographies of clean and adsorbate-covered surfaces.^{1,2} In order to relate the diffraction data to specific surface structures, it is necessary to know the He surface potential and its dependence on surface geometry. Although the weakly attractive region of several surface potentials has been determined with some accuracy by analyzing scattering resonances,³ there is considerable uncertainty about the repulsive region which dominates the diffraction pattern. The repulsion arises from the overlap of the He electrons with the tail of the surface charge distribution. Recent theoretical considerations^{4,5} suggest that (to first order) this repulsion is simply proportional to the surface charge density $\rho(\mathbf{r})$:

$$V(\mathbf{r}) = \alpha \rho(\mathbf{r}) \quad (1)$$

where \mathbf{r} denotes the position of He atom and α is a constant which has been estimated to lie between 300 and 700 eV a.u.⁴⁻⁷ Equation (1) implies that surfaces of constant charge density are essentially isopotential surfaces for He atoms, and the classical surface of closest approach (CA) corresponds to $\rho_{CA} = E_i/\alpha$ where E_i is the energy of the incident He atom. Typically $E_i \sim 30$ meV so that $\rho_{CA} \sim 5 \times 10^{-5}$ a.u. Although first-principles calculations of $\rho(\mathbf{r})$ at these very low densities have been carried out,⁸ they require substantial computational effort and are restricted in the size of the unit mesh which can be handled. A simplifying approximation for $\rho(\mathbf{r})$ is commonly used, spherical atomic charge superposition, which expresses $\rho(\mathbf{r})$ as a sum of atomic charge densities⁹⁻¹² ρ_{at}

$$\rho(\mathbf{r}) = \sum_i \rho_{at}(|\mathbf{r} - \mathbf{r}_i|), \quad (2)$$

where \mathbf{r}_i represents the position of i th atom on the surface. In this case, the total He surface potential of Eq. (1) becomes a summation of contributions from each atom, analogous to the summation of a pairwise potential. A combination of Eq. (1) and Eq. (2) provides a simplified

way to analyze He diffraction data and has been applied to a variety of surfaces. Although the discussion about the validity and modifications to Eq. (1) continues,¹³ a more serious error may often be contained within the simplified procedures used to generate surface charge densities. There is no microscopic justification for the additivity of atomic charges.

In this paper we test atomic charge superposition for the Si(100) surface assuming a tilted dimer structural model. We use the linear-augmented-plane-wave (LAPW) method to calculate self-consistent charge-density surfaces⁸ for two periodicities, the 2×1 and $c(2 \times 2)$, using the same local dimer geometry in both cases. We find simple spherical charge superposition inadequate. We develop a modified atomic charge superposition (MACS) scheme which allows for surface atoms of different "size" and charge anisotropy. With this procedure we approximate the potential region for the thermal He surface interaction quite well.

Our underlying motivation in this study is to utilize He diffraction as a probe of the topography of the Si(100) surface. Previous experimental¹⁴⁻¹⁶ and theoretical¹⁷⁻¹⁹ results suggest that the equilibrium periodicity of Si(100) is $c(4 \times 2)$, but that it is easily disordered at room temperature. To compare structural models based on He diffraction analysis, charge densities for the $c(4 \times 2)$ periodicity are required. However the $c(4 \times 2)$ unit mesh is too large to be treated by the LAPW method within the present limits of our computational capacity, so approximation schemes are necessary. In order to confidently utilize the MACS scheme that we develop here for different structures, we test the transferability of its underlying parameters. For a buckled dimer structural model¹⁹ we fit our MACS scheme to the LAPW charge densities of Si(100) 2×1 , and then check the fit to the LAPW charge densities of the $c(2 \times 2)$ structure using the same parameters. We also compare the He diffraction spectra calculated from the MACS and LAPW surfaces. Based on these successful comparisons we make use of the MACS to compare both $c(4 \times 2)$ and 2×1 periodicities of buckled dimer models to previously obtained experimental results.¹⁶

TABLE I. Corrugation heights of two charge-density surfaces based on the LAPW, simple spherical charge superposition (SCS), and MACS technique.

Charge density (a.u.)	Corrugation height (\AA)				
	LAPW	Si(100) 2×1 SCS	MACS	Si(100) $c(2\times 2)$ LAPW	MACS
3.0×10^{-5}	1.61	0.93	1.63	1.36	1.33
1.0×10^{-4}	1.69	1.08	1.70	1.49	1.58

II. CHARGE-DENSITY CALCULATIONS

A. LAPW calculation

Self-consistent surface charge densities were calculated for a four-layer slab of Si(100) using the LAPW method.⁸ The dimer configuration proposed by Yin and Cohen¹⁹ was employed in the calculation, but the displacements of the second-layer atoms were neglected for simplicity. Charge densities of 10^{-6} – 10^{-1} a.u. were obtained for 2×1 and $c(2\times 2)$ periodicities, and their cross sections are plotted in Fig. 1. Note that at ~ 5 \AA above the surface the charge contours of Si(100) are still highly corrugated and resemble the shape of the surface dimer. The peak-to-trough heights are tabulated in Table I for contours of 1.0×10^{-4} and 3.0×10^{-5} a.u. which correspond [via Eq. (1)] to typical He energies used in the diffraction experiments.¹⁶

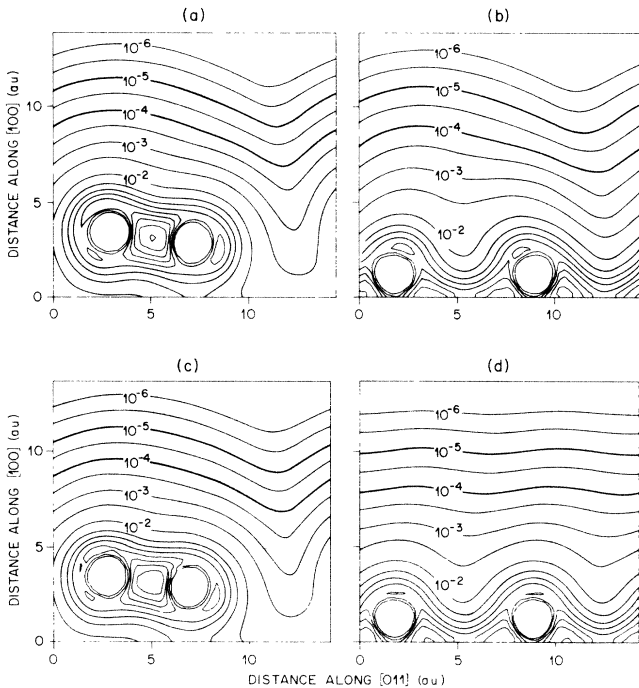


FIG. 1. LAPW surface charge contours of Si(100) 2×1 [(a) and (b)], and Si(100) $c(2\times 2)$ [(c) and (d)]. In both cases, the cross-sectional view is shown for the $(0\bar{1}1)$ plane containing the dimer atoms [(a) and (c)], and for the $(0\bar{1}\bar{1})$ plane containing second-layer atoms [(b) and (d)]. The Yin-Cohen dimer geometry¹⁹ is used in the calculation. Contours are spaced logarithmically in the vacuum region (10^{-6} , 3×10^{-5} a.u., etc.) and then linearly (0.01, 0.02 a.u., etc.).

There is a strong similarity between charge contours of 2×1 and $c(2\times 2)$ periodicities in the cut which contains the dimer bond [Figs. 1(a) and 1(c)]. This similarity indicates that the chemical bonding of the surface dimers is similar in detail for these periodicities, as well as the fact that the dimer registration along this direction is the same. On the other hand, there is a phase shift in the dimer registration of the $c(2\times 2)$ surface. This reduces the corrugation in the region between dimer lines compared to the 2×1 surface so that the contours in Fig. 1(d) are quite different from those in Fig. 1(b). Thus there is sensitivity of the overall corrugation profiles in the charge contours to the dimer registration or the surface periodicity.

B. Spherical charge superposition

Charge-superposition calculations were performed for Si(100) with the same surface structure as used above in the LAPW method. The atomic charge density ρ_{at} in Eq. (2) was assumed to have the form,

$$\rho_{\text{at}}(r) = \rho_0 e^{-\kappa r} / \kappa r, \quad (3)$$

where $\kappa = 2.29 \text{ \AA}^{-1}$ and $\rho_0 = 1.7$ a.u. were determined from the self-consistent charge distribution of the Si atom in the sp^3 configuration.²⁰ This approximate form was fit to match the value and the slope of self-consistent charge densities at a radius in the range of interest here. In Fig. 2 we show the cross-sectional view of the charge contours obtained from Eqs. (2) and (3). There is a qualitative similarity between the contours of this charge superposition and those of the LAPW. However, the quantitative agreement is poor as can be seen in Fig. 3 where we have superimposed the results of these two methods. The largest discrepancy is around the contour minima: the

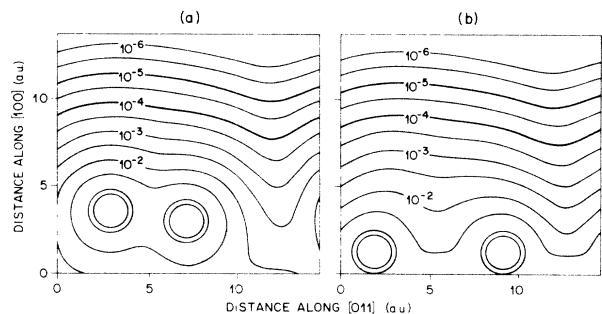


FIG. 2. Surface charge contours of Si(100) 2×1 obtained from the simple charge superposition. The dimer geometry is the same as in Fig. 1.

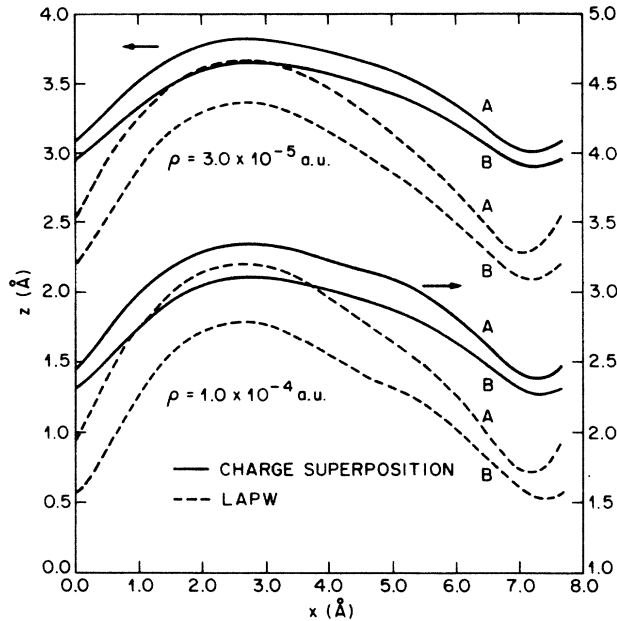


FIG. 3. Comparison of the charge contours of Si(100) 2×1 obtained from the LAPW (dashed line) and from the simple charge superposition (solid line) at two charge densities. For each contour, two cross sections are shown: (a) cut through the (0 $\bar{1}$ 1) plane containing dimer atoms, (b) cut through the (0 $\bar{1}$ 1) plane passing through the second-layer atoms. Note that the contours at 1.0×10^{-4} a.u. refer to the scale at the right-hand side.

LAPW contours have much deeper minima. At $\rho = 1.0 \times 10^{-4}$ a.u., this discrepancy gives rise to a difference of 0.6 Å in the peak-trough corrugation, which amounts to about 35% of the total corrugation. It is clear from this comparison that simple charge superposition cannot be used for analysis of the He diffraction data from Si(100). We note that the comparison in Fig. 3 indicates an overestimation of the charge contribution from the “down” atom in the buckled dimer. We explore this in Fig. 4 where we plot the decay of the charge density along the surface normal at the position of the “up” atom [Fig. 4(a)] and at the “down” atom [Fig. 4(b)]. Above the down atom, the LAPW charge density is always smaller than the charge-superposition value. Thus the down atoms effectively appear “smaller” than the up atoms for which the LAPW and the charge superposition show a similar decay behavior. We note that an asymmetry in the charge distribution of buckled dimers on Si(100) has been calculated by Ihm *et al.*¹⁸ While they did not consider the low-charge-density region studied here, their asymmetry is consistent with our results.

C. Modified atomic charge superposition (MACS)

The above arguments suggest a modification of the simple charge-superposition scheme to allow for different atomic charge distributions for the two dimer atoms. The necessity for such a modification was indicated by Laugh-

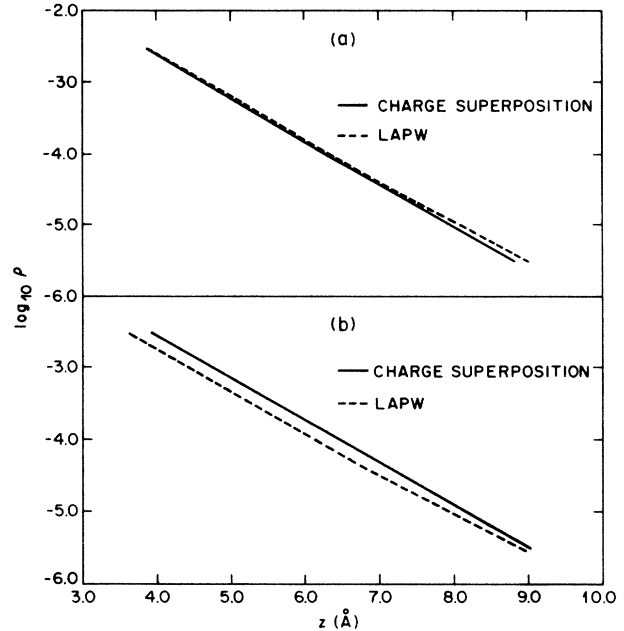


FIG. 4. Decay behavior of the calculated surface charge densities of Si(100) 2×1 . The horizontal scale measures the distance from the up atom (a) or from the down atom (b).

lin⁵ in his analysis of the He scattering potential of GaAs(110). To obtain reasonable agreement with He diffraction, the longer-ranged Ga atomic charge was neglected and extra charge assigned to As, consistent with the physical origin of charge transfer which is the buckling on that surface. The highest occupied electronic state on this surface is a surface state with its weight concentrated on As atoms. In the case of Si(100), however, there is no simple argument which allows a quantitative assignment of an appropriate atomic charge distributions around each of the dimer atoms. Accordingly, we have determined atomic charge distribution parameters from a least squares fit to the LAPW charge contours.

The following procedure was employed in the fitting calculation: We divided Si atoms into three kinds depending on their positions. Atoms I and II refer to the up and the down atoms of the buckled dimer, respectively, and atom III represents all other bulklike atoms in the deeper layers. These three kinds of atoms were assumed to have the following charge-distribution function but with different parameters,

$$\rho_{at,i}(x,y,z) = \rho_{0i} \exp[-\kappa_i(r-r_0)] , \quad (4)$$

$$r = [(x-x_a)^2 + (y-y_a)^2 + (z-z_a)^2(1-\beta_i^2)]^{1/2} ,$$

where (x_a, y_a, z_a) is the position of nucleus and $\rho_{0i}, \kappa_i, \beta_i$ ($i=I,II,III$) are fitting parameters. Unlike the previous charge density of Eq. (3), we adopted the form of a simple exponential decay. In addition to the decay constant κ_i and the prefactor ρ_{0i} , we found it necessary to introduce a third parameter β_i in Eq. (4) which describes a nonsphericity of the charge distribution. The charge density around

each atom becomes prolate or oblate for $\beta_i > 0$ or $\beta_i < 0$, respectively. A fixed constant $r_0 = 7.4454$ a.u. was used in Eq. (4) in order to avoid large changes in ρ_{0i} during the fitting computation caused by small changes in κ_i .

The total charge density is then expressed as a sum of contributions from all atoms,

$$\rho(\mathbf{r}) = \sum_{i=I,II,III} \rho_{at,i}(\mathbf{r}) \quad (5)$$

and the surface of constant charge density $\xi(x,y)$ at $\rho = \rho_c$ is given by the equation $\rho(x,y,\xi(x,y)) = \rho_c$. Because of the large corrugation of these surfaces, it is not desirable to fit a volume charge density in some simply defined box since this gives too much weight to charge densities irrelevant for He diffraction. Fitting the functions $\xi(x,y)$ is too inefficient computationally, since it involves repeated solution of the implicit equation $\rho(x,y,\xi) = \rho_c$. Instead, we carried out what is in effect a "maximum relevancy" volume fit, evaluating trial superposition densities on several LAPW surfaces $\xi_{LAPW}(x,y)$ and minimizing

$$\sum_{x,y} |\ln \rho[x,y,\xi_{LAPW}(x,y)] - \ln \rho_c|^2, \quad (6)$$

where $\ln \rho$ is used rather than ρ to equalize the weight on the desired contours. The summation in Eq. (6) was carried out over 20×10 mesh points in the 2×1 unit cell.

We found that the relevant charge contours are quite insensitive to the parameters of the second-layer atoms (atom III), but critically dependent on the nuances of the atomic charge distributions of dimer atoms (atoms I and II) including the anisotropy ($\beta_i \neq 0$). Since the weak dependence on ρ_{0III} and κ_{III} caused computational instability, we first optimized the parameters of dimer atoms and then determined ρ_{0III} and κ_{III} independently. We fixed $\beta_{III} = 0$ throughout the calculation.

The fitting calculations were performed for the 2×1 periodicity for two LAPW surfaces of constant charge; $\rho = 1.0 \times 10^{-4}$ a.u. and $\rho = 3.0 \times 10^{-5}$ a.u. The resulting values of the parameters are summarized in Table II. Charge contours generated using the optimized parameters are plotted and compared with the LAPW contours in Fig. 5. Although there remains a small discrepancy around the minimum point, the overall fit is excellent. The peak-to-trough heights derived from these contours are in good agreement with the LAPW values as seen in Table I: differences are within 0.05 \AA .

TABLE II. Optimized values of the parameters of Eq. (4).

Parameter	Optimized value (a.u.)
κ_I	1.520
κ_{II}	1.451
κ_{III}	2.267
ρ_{0I}	7.30×10^{-6}
ρ_{0II}	5.48×10^{-6}
ρ_{0III}	2.58×10^{-6}
β_I	9.19×10^{-2}
β_{II}	4.16×10^{-2}
β_{III}	0.0 (fixed)

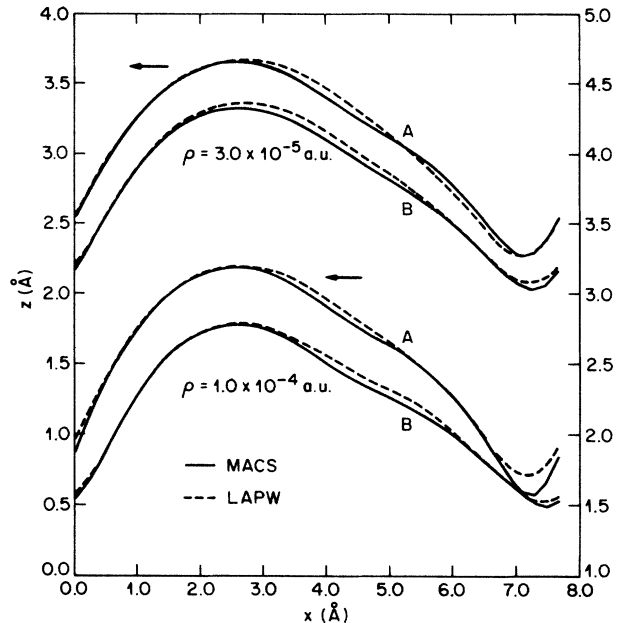


FIG. 5. Comparison of the charge contours of Si(100) 2×1 obtained from the LAPW (dashed line) and MACS (solid line). Symbols and scales are the same as in Fig. 3.

To further establish the validity of the MACS, we test whether the values of the parameters in Table II are specific to the 2×1 periodicity. For the same buckled dimer model we calculate surfaces of constant charge density of Si(100) $c(2 \times 2)$ using the MACS with the parameters of Table II. In Fig. 6 we compare the resulting contours at two charge densities with the corresponding LAPW contours. The agreement is quite satisfactory. The differences in the corrugation height are slightly

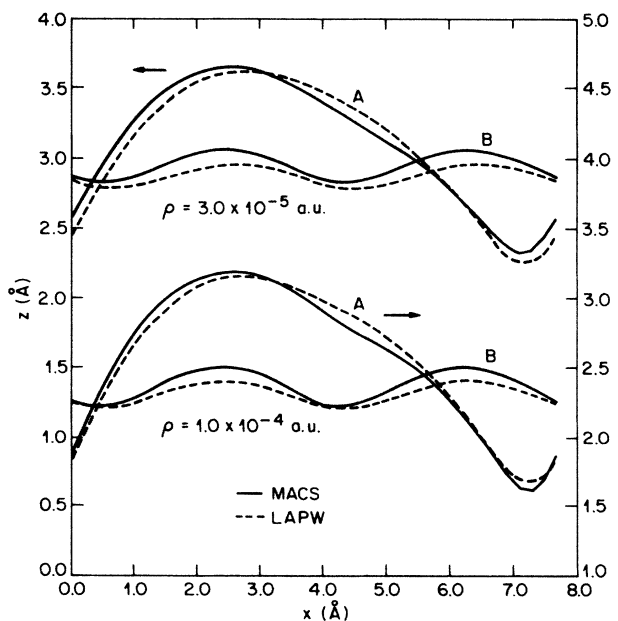


FIG. 6. Same as Fig. 5 but for Si(100) $c(2 \times 2)$.

larger than the case of the 2×1 , but they are still less than 0.1 Å (Table I). Based on this agreement, the MACS scheme appears to be a viable procedure for the generation of charge densities required for He diffraction analysis. The appropriate test, however, is the comparison of diffraction spectra, which are calculated below.

III. DISCUSSION

A. Atomic charge density

In Table II, the decay constants of the atomic charge density of dimer atoms (κ_I and κ_{II}) are smaller than that of bulklike atoms (κ_{III}), indicating that the charge density around the dimer is more weakly bound. The value of κ_{II} is slightly smaller than κ_I . Although this appears to contradict the results in Fig. 4 which show the larger effective size of the up atom, we note that the decay constant along the surface normal direction is not κ_i but $(1-\beta_i)\kappa_i$ which is 1.38 a.u.⁻¹ for up atoms and 1.39 a.u.⁻¹ for down atoms, respectively. This result, combined with the fact that the value of ρ_{OI} is larger than ρ_{OII} , shows that more charge is concentrated around the up atom and it extends along the surface normal direction.

This result is consistent with the predicted electronic structure of the buckled dimer. Chadi¹⁷ reported that the buckling is associated with the charge transfer from down atoms to up atoms. The highest occupied states of this surface are a π -bonding combination of the single remaining dangling bond in each dimer atom. Buckling polarizes this π bond towards the up atom and makes the effective size of up atoms larger than that of down atoms. In addition, the directionality of the dangling bonds results in an anisotropic charge distribution elongated in the surface normal direction. The effective "average atomic energy" of deeper layer atoms, which have no dangling bonds, is well below the valence band maximum, so their charges decay rapidly and they are the "smallest" atoms.

Note that the electronic structure of Si(100) as described above is well represented by parameters in Table II. Particularly the relatively large positive value of the anisotropic factor β_I is consistent with the nonspherical charge distribution due to dangling bonds since the positive β_I correctly gives a prolate charge contour oriented along the surface normal direction. The physical plausibility of the MACS parameters is an interesting aspect of this scheme.

B. Surface periodicity and the He scattering potential

Previous studies, including He diffraction,¹⁴⁻¹⁷ have suggested that the major surface periodicity of Si(100) is (disordered) $c(4 \times 2)$, and not 2×1 as is commonly assumed. We thus use the parameters of Table I, verified as to their transferability, to generate $c(4 \times 2)$ charge densities to enable a comparison with the He diffraction experiment. In Fig. 7 we show the calculated peak-to-trough heights of the corrugation profiles for various periodicities including $c(4 \times 2)$. They are plotted as a function of charge density so that the uncertainty in the proportional constant in Eq. (1) can be considered. A strong depen-

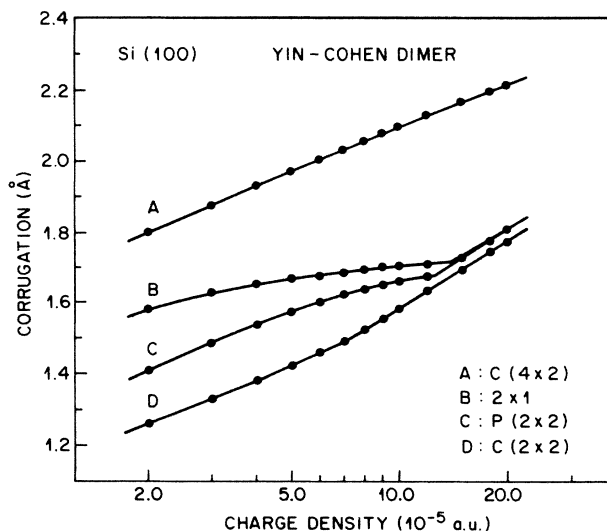


FIG. 7. Corrugation heights of Si(100) calculated using the MACS for various surface periodicities. An abrupt increase of the corrugation above 1.5×10^{-4} a.u. for the 2×1 and $p(2 \times 2)$ structures is due to a change in the location of the corrugation minimum.

dence of corrugation height on periodicity is evident in the figure. The $c(4 \times 2)$ gives the largest corrugation, and the difference in corrugation with other periodicities amounts to more than 0.2 Å for 2×1 and more than 0.5 Å for $c(2 \times 2)$. Note, however, that corrugation heights are at best a crude indication of the comparability of scattering potentials. Comparison of the diffraction spectra is the most appropriate test of the differences between potentials. The principal features of He diffraction spectra, such as rainbow maxima and supernumeraries, depend upon the detailed shape of the charge densities. We employ the eikonal approximation²¹ to calculate He diffraction spectra and compare results from the MACS and the LAPW. We take charge-density surfaces at 1.0×10^{-4} and 3.0×10^{-5} a.u. as hard-wall scattering potentials for several incident angles. The He wavelength was fixed at 0.98 Å, and a refraction correction for the effect of the attractive potential D was included with $D=6.8$ MeV, which was estimated from the potential function formulated by Laughlin.⁵

The combination of the eikonal and corrugated hard-wall approximations may not be appropriate for a quantitative comparison with experiment for highly corrugated surfaces like Si(100). However, it gives the correct principal features of He diffraction spectra in general,²¹ and it is sufficient for the purpose of comparing two scattering potentials.

The diffraction calculations were carried out for both 2×1 and $c(2 \times 2)$ periodicities, and the results are shown in Fig. 8 for the MACS and the LAPW surfaces at $\rho=3.0 \times 10^{-5}$ a.u. In this figure, the calculated spectra at incident angles $\theta_i=30^\circ, 50^\circ$, and 70° are plotted for three incident azimuth angles $\phi_i=0^\circ, 90^\circ$, and 180° . Note that the Si(100) has a two-domain structure. The diffraction spectra at $\phi_i=0^\circ, 90^\circ$, and 180° represent the domain con-

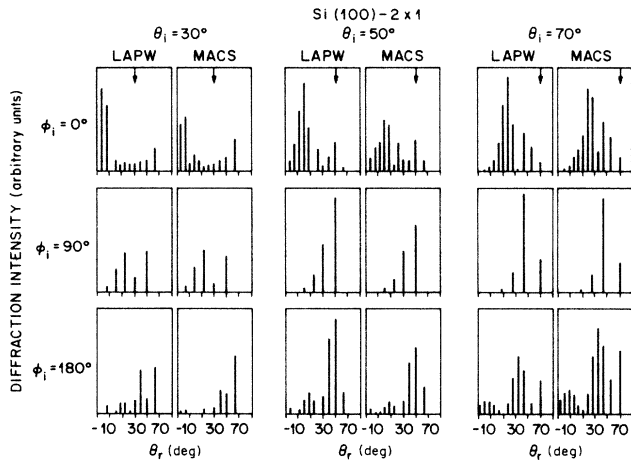


FIG. 8. Calculated diffraction spectra from LAPW and MACS charge density of Si(100) 2×1 at 3.0×10^{-5} a.u. The results at three incident angles and three azimuth angles are shown in the figure. The azimuth angles correspond to the orientations of the domains of Si(100) 2×1 .

tributions to the experiment (270° domains are equivalent to 90° domains).

In Fig. 8, we note there is excellent agreement between the diffraction spectra from the MACS and the LAPW contours. There is at most a one-beam difference in the position of the intensity maximum in the 0° domain spectra at 30° and 70° , but in all other spectra the envelopes of the diffraction intensities are in perfect correspondence. The small discrepancy of the position of intensity maximum (rainbow maximum) in Fig. 8(a) at 70° shows that the MACS surface is slightly more steeply corrugated than the LAPW (see Table I). Although the one-beam shift of the rainbow maximum at only one angle of incidence is a minor difference, it demonstrates the sensitivity of the diffraction spectra to the detailed shape of the charge surfaces. Good agreement was also obtained for charge densities of 1.0×10^{-4} a.u. thereby confirming the essential equivalence of the MACS and the LAPW for Si(100) 2×1 *vis-à-vis* He diffraction.

In Fig. 9 we compare the diffraction spectra obtained

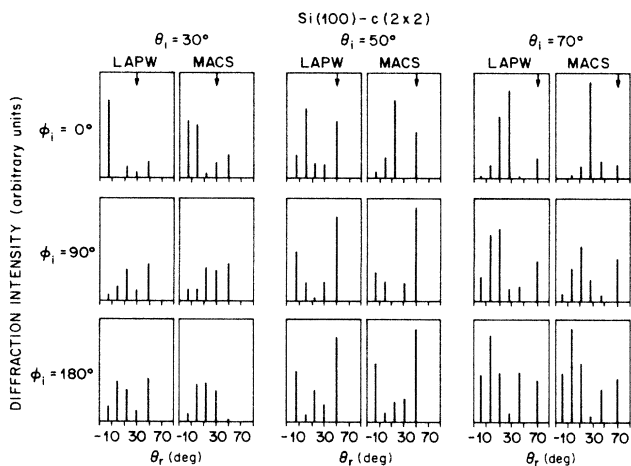


FIG. 9. Same as Fig. 8 but for Si(100) $c(2 \times 2)$.

for the $c(2 \times 2)$ periodicity. The agreement here between the results of the MACS and LAPW is not as good as for the 2×1 but still acceptable. In the 0° domain, the diffraction from the MACS has an intensity maximum around the $(\bar{2}0)$ beam, whereas it appears around $(\bar{3}0)$ beam in the spectra from the LAPW. This shift of the rainbow maximum is again consistent with the steepness of the corrugation (Table I) which is greater for the LAPW of the $c(2 \times 2)$. In addition, a supernumerary is seen in the LAPW diffraction spectra from the 180° domain at 50° but is almost collapsed into the specular in the case of the MACS, again indicating a less steep corrugation of the MACS. In spite of these differences, the two series of spectra in Fig. 9 have many common features: the diffraction from the 90° domain is essentially the same for MACS and LAPW, and the correspondence of the rainbow position is perfect for the diffraction from the 180° domain. In summary, the agreement of the diffraction spectra for the $c(2 \times 2)$ is quite acceptable, and indicates that the transferability of MACS to other periodicities of this structural model is appropriate if the analysis is restricted to the principal features of the diffraction patterns, i.e., rainbow and supernumerary rainbow positions.

C. Comparison with experiment

He diffraction spectra from Si(100) show diffuse intensity maxima around the quarter-order positions associated with $c(4 \times 2)$ periodicity, but no sharp diffraction beams on which to base an analysis. The basic 2×1 reconstruction, pairing, has long-range coherence, presumably enforced by the large energy cost of defects in this structure (broken dimer bonds). The fourth-order superstructure, tentatively associated with tilting, presumably has a much smaller ordering energy and many defects. The local geometry associated with these distortions is represented in the intensity distributions of the integer and half-order diffraction beams, however, so it is valid to compare 2×1 and $c(4 \times 2)$ structures on this basis.

The experimental He diffraction spectra from Si(100) for the incident angular range $\theta_i = 50^\circ - 70^\circ$ are shown in Fig. 10. Also shown are the theoretical spectra obtained by MACS eikonal calculation for Si(100) 2×1 and $c(4 \times 2)$. In these calculations the uniform refracting well depth is $D = 6.8$ MeV and we have used $\alpha = 675$ eV a.u. for the proportionality constant in Eq. (1). The charge density corresponding to the classical turning point of He atom with 0.98 \AA wavelength is $\rho = 4.2 \times 10^{-5}$ a.u. This charge-density surface was calculated and used as a hard-wall potential. We averaged the diffraction intensity over the domain orientations with equal weight for each domain.

In Fig. 10 we first note that in the experimental data there is a backscattered rainbow maximum which occurs around $\theta_r \sim -15^\circ$ for $\theta_i = 70^\circ$ and moves to $\theta_r = -20^\circ$ at $\theta_i = 60^\circ$ and beyond $\theta_r = -20^\circ$ for $\theta_i = 50^\circ$. This rainbow smoothly includes half- and integer-order beams and therefore arises from the half-order direction (along the dimer bond). The calculated rainbows for the $c(4 \times 2)$ structure agree exactly with this feature over this incident

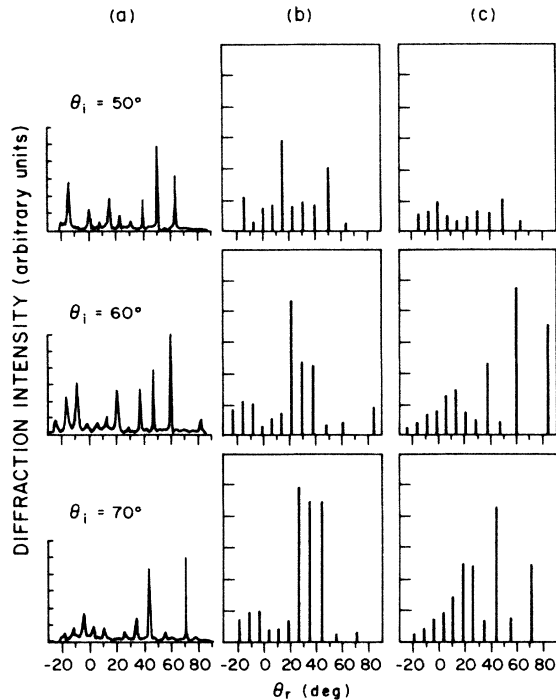


FIG. 10. Experimental diffraction spectra from Si(100) (a), and calculated spectra from the MACS of Si(100) $c(4 \times 2)$ and 2×1 [(b) and (c)]. In the calculation, a charge density of 4.2×10^{-5} a.u. was used, and the results were averaged over possible domain orientations.

angle range. In contrast the corresponding rainbow for the 2×1 appears considerably closer to the specular beam, indicative of a substantially less steep corrugation profile. We note however that the observed rainbow in the 2×1 spectra arises from only one of the half-order domain directions. The tilted dimer has no mirror plane of symmetry and thus one direction along the tilted dimer bond is more steeply corrugated than the other [like GaAs(110) (Ref. 22)]. Scattering from the steeper profile also results in a rainbow maximum, but at very distant backscattering angles and with very little intensity, so that it is not observed on the scale of this plot. The increase in the slope of the steep side of the 2×1 corrugation profile results in considerably reduced in-plane scattering power. Consequently the less steep direction of the 2×1 tilted dimer dominates the scattering from the half-order domains.

Another feature of the experimental data is a maximum closer to the specular beam, occurring in beams 2–4 at $\theta_i = 70^\circ$. It moves farther from the specular beam as $\theta_i \rightarrow 50^\circ$ and appears to contribute more to the integer beams than the half-order beams. We interpret this feature as a rainbow from the integer direction. This interpretation was assisted by separate domain calculations. This feature is also in good agreement with the calculated spectra from the $c(4 \times 2)$ but not in accord with the 2×1 calculations.

To account for the uncertainty in the value of the potential well depth, we have also calculated the diffraction spectra from the 2×1 periodicity using a much deeper at-

tractive well, $D=20$ MeV. We find that the rainbows move outward due to the expected increased refraction, compared to the results in Fig. 10, but they are still too close to the specular beam indicating that the experiment and the calculated 2×1 spectra cannot be reconciled by increasing the well depth.

These arguments are made for the incident angular range $50 \leq \theta_i \leq 70^\circ$. At more normal incidence the simple and direct interpretation of both the experimental and calculated diffraction spectra is no longer possible.

We have compared the $c(4 \times 2)$ and 2×1 periodicities for other tilted dimer models.^{17,23,24} In general the different dimer structures do not result in sufficiently different calculated diffraction patterns for a particular periodicity so that they can be assessed at this level of analysis. However, for all cases the difference between $c(4 \times 2)$ and 2×1 is sufficient that the $c(4 \times 2)$ can be clearly preferred.

An extreme case of the $c(4 \times 2)$ dimers is the symmetric dimer which is relatively smooth (peak-trough corrugation ~ 1 Å) and easily excluded. In the other direc-

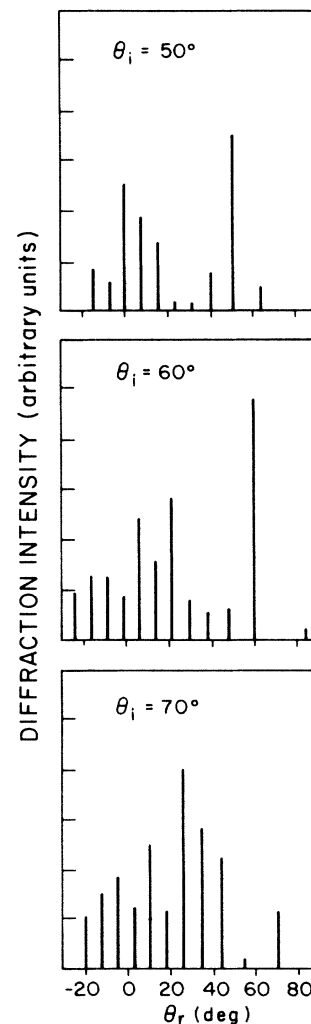


FIG. 11. Calculated diffraction spectra from Chadi dimers (Ref. 17) in the $c(4 \times 2)$ registration.

tion the dimer geometry proposed by Chadi¹⁷ has a larger buckling angle and more steeply corrugated potential than the model we have just considered. We have calculated the diffraction spectra for the Chadi $c(4\times 2)$ structure and show the results in Fig. 11. The half-order rainbow and half-order supernumerary positions are in acceptable agreement with the data. However the rainbow maximum from the integer direction is farther from specular than in either the data or in the Yin-Cohen geometry (Fig. 10) as expected for a surface more steeply corrugated. The dimer geometry proposed by Tromp *et al.*²³ shows similar diffraction spectra to Chadi's. However, there are sufficient uncertainties at this level of analysis that these two dimer structures in a $c(4\times 2)$ arrangement can not be ruled out although they are not preferred.

Finally we comment on the recent "dimer-plus-chain" model proposed by Northrup.²⁵ We have also carried out eikonal calculations for this model. We have tried several assignments of MACS parameters to the chain atoms in the absence of an LAPW calibration. Although we do not consider this a comprehensive test, we find that in general the dilute charge-density surfaces of the Northrup model are quite flat along symmetry directions parallel to the chain. This results in negligible scattering power in the diffraction beams (except the specular) from the integer domains. This result is in serious disagreement with the He diffraction experiments, which show significant diffraction contributions at large Δk_{\parallel} from the integer domains.

IV. SUMMARY

We find simple spherical charge superposition, with the same charge distribution for all atoms, incapable of generating a He scattering potential for tilted dimer models of the Si(100) surface. Using *ab initio* LAPW results for calibration, we develop a modification of the simple charge superposition to allow for atomic size differences and anisotropy. With this scheme we accurately fit the dilute charge densities around the dimer atoms for the 2×1 periodicity. We show that the derived parameters from this 2×1 fit reproduce the dilute LAPW charge densities of the $c(2\times 2)$ structure. The charge densities we obtain are physically consistent with what is known of the electronic structure of the buckled dimer, extended to the dilute region of our comparison. We test the MACS scheme against the LAPW using He diffraction spectra as a measure. As an application of the MACS, we calculate the He diffraction spectra for the 2×1 , $c(2\times 2)$, and $c(4\times 2)$ periodicities of Si(100) for several models of tilted dimers. We find that the $c(4\times 2)$ periodicity is strongly preferred for a range of dimer models from the comparison of the calculated spectra with experiment.

ACKNOWLEDGMENTS

The authors acknowledge J. Tersoff for calculations and stimulating discussions of the spherical atomic charge superposition.

*On leave from the Institute for Solid State Physics, The University of Tokyo 7-22-1 Roppongi, Minato-ku, Tokyo 106, Japan.

¹T. Engel and K. H. Rieder, in *Structural Studies of Surfaces*, Vol. 91 of *Springer Tracts in Modern Physics*, edited by G. Hohler (Springer, Berlin, 1982).

²M. J. Cardillo, in *Chemistry and Physics of Solid Surfaces IV*, edited by R. Vanselow and R. Howe (Springer, Berlin, 1982).

³M. W. Cole, D. R. Frankl, and D. L. Goodstein, *Rev. Mod. Phys.* **53**, 199 (1981).

⁴N. Ejsberg and J. K. Nørskov, *Phys. Rev. Lett.* **45**, 807 (1980).

⁵R. B. Laughlin, *Phys. Rev. B* **25**, 2222 (1982).

⁶J. Harris and A. Liebsch, *J. Phys. C* **15**, 2275 (1982).

⁷M. Manninen, J. K. Nørskov, M. J. Puska, and C. Umrigar, *Phys. Rev. B* **29**, 2314 (1984).

⁸D. R. Hamann, *Phys. Rev. Lett.* **46**, 1227 (1982).

⁹D. Haneman and R. Haydock, *J. Vac. Sci. Technol.* **21**, 330 (1982).

¹⁰N. Garcia, J. A. Barker, and I. P. Batra, *Solid State Commun.* **47**, 485 (1983).

¹¹I. P. Batra, *Surf. Sci.* **148**, 1 (1984).

¹²M. Manninen, J. K. Nørskov, and C. Umrigar, *J. Phys. F* **12**,

L7 (1982).

¹³(a) J. F. Annett and R. Haydock, *Phys. Rev. B* **29**, 3773 (1984); (b) Y. Takada and W. Kohn, *Phys. Rev. Lett.* **54**, 470 (1985); (c) J. Tersoff, *ibid.* **55**, 140 (1985).

¹⁴J. J. Lander and J. Morrison, *J. Chem. Phys.* **37**, 729 (1962).

¹⁵T. D. Poppendieck, T. C. Ngoc, and M. B. Webb, *Surf. Sci.* **75**, 287 (1978).

¹⁶M. J. Cardillo and G. Becker, *Phys. Rev. B* **21**, 1497 (1980).

¹⁷D. J. Chadi, *Phys. Rev. Lett.* **43**, 43 (1979), *J. Vac. Sci. Technol.* **16**, 1290 (1979).

¹⁸J. Ihm, M. L. Cohen, and D. J. Chadi, *Phys. Rev. B* **21**, 4592 (1980).

¹⁹M. T. Yin and M. L. Cohen, *Phys. Rev. B* **24**, 2303 (1981).

²⁰J. Tersoff (unpublished).

²¹U. Garibaldi, A. C. Levi, R. Spadacini, and G. E. Tommei, *Surf. Sci.* **48**, 649 (1975).

²²M. J. Cardillo, G. E. Becker, S. J. Sibener, and D. R. Miller, *Surf. Sci.* **107**, 469 (1981).

²³R. M. Tromp, R. G. Smeenk, F. W. Saris, and D. J. Chadi, *Surf. Sci.* **133**, 137 (1983).

²⁴J. Ihm (unpublished).

²⁵J. E. Northrup, *Phys. Rev. Lett.* **54**, 815 (1985).